JOURNAL OF KUFA–PHYSICS
www.uokufa.edu.iq/journals/index.php/jkp | ISSN: 2077–5830

Variable Optical Buffer Using EIT in Three Level System Based on Semiconductor Conical Quantum Dots

Nooralhuda S.Yaqoob * **Sabah M.M. Ameen**

Physics Dept., College of Science, University of Basrah, Basrah, Iraq .

*Corresponding Author E-mail: sabah644@yahoo.com

ARTICLE INF

Article history:
Received: 12 JAN, 2019
Accepted: 18 MAY., 2020
Available Online: 25 SEP, 2020

Keywords:

Electromagnetically induced transparency
Semiconductor Conical Quantum Dots
Variable Optical Buffer

ABSTRACT

A variable semiconductor optical buffer based on the electromagnetically induced transparency (EIT) in a three level conical quantum dot system (CQD) is theoretically investigated. The system is interacting with two (control and signal) laser beams. Signal light with subluminal velocity is possible in such system through the quantum interference effect induced by the control pump field. We investigate the refractive index and absorption spectra of the QD waveguide at different pump levels, which exhibit an optimal pump power for maximum slow-down factor (SDF). The group velocity SDF is theoretically analyzed as a function of the pump intensity at different broadened linewidths. The present study is based on the assumption that the medium is homogeneous. In this paper, a SDF as a function of CQD radius was studied. The simulation results indicate that the SDF increases with decreasing CQD radius.

DOI: http://dx.doi.org/10.31257/2018/JKP/2020/120108

استعمال الشفافية المحتثة كهرومغناطيسيا في نظام النقاط الكمية المخروطية شبه الموصلة ذات الثلاث مستويات لتحقيق المبطئ البصري المتغير

نور الهدى صالح يعقوب **د. صباح مهدي محمدأمين**

قسم الفيزياء، كلية العلوم، جامعة البصرة، البصرة، العراق

الكلمات المفتاحية:

استعمال الشفافية المحتثة كهرومغناطيسيا
النقاط الكمية المخروطية شبه الموصلة
المبطئ البصري المتغير

الـــخُـــلاصـــة

في هذا البحث أجريت دراسة نظرية للمبطئ البصري المتغير المستند على ظاهرة الشفافية المحتثة كهرومغناطيسيا EIT في انظمة النقاط الكمية المخروطية الشكل CQD ذات الثلاث مستويات. يتفاعل هذا النظام الكمي مع شعاعين ليزريين هما الاشارة والسيطرة. من المعروف ان ليزر الاشارة يعاني ابطا في سرعته (في حالة عدم وجود ليزر ضخ) عند مروره في هذه الاوساط وكذلك تنخفض شدته بسبب الامتصاص من قبل الوسط. في حالة تعريض الوسط لليزر ضخ تحدث ظاهرة التداخل الكمي بين الانتقالات التي يحدثها الضخ. تحت

ظروف معينة يحدث تداخل كمي اتلافي بين هذه الانتقالات وبذلك يكون الوسط شفاف ولا يعاني ليزر الاشارة من الامتصاص وتنخفض سرعتها بشدة. درس طيف معامل الانكسار (وهو مؤشر لسرعة الاشارة) والامتصاص لهذا النظام لمعرفة افضل قدرة ضخ تؤدي لاقصى معامل ابطاء .SDF حسب معامل الابطاء نظريا كدالة لشدة الضخ ولقيم مختلفة من عرض خط مستوى طاقة الانتقال. افترضت الدراسة تجانس هذه الاوساط. درس كذلك معامل الابطاء كدالة لنصف قطر النقطة الكمية. أظهرت الدراسة ان معامل الابطاء يزداد كلما قل نصف قطر النقطة الكمية.

1. INTRODUCTION

An optical memory with controllable variable storage time is one of the most critically components in optical communications and signal processing [1-5]. Where, one of the crucial components is the realization of all-optical packet-switched networks based on variable optical buffers. In such a buffer, the optical signal would be remained in the optical field during the storage time without being transformed into an electronic field [6]. The buffer must be able to switch on to store/delay and off to release the optical data at a very rapid rate by an external optical controlling field. The buffer storage time can be adjusted to desired values via controlling the group velocity decreasing factor. Several methods are used for decreasing the light velocity, these includes Electromagnetically Induced Transparency (EIT), Coherent Population Oscillation (CPO), Stimulated Brillouin scattering (SBS) and Stimulated Raman scattering (SRS) [7-9]. EIT is a spectral region of transparency created in the resonant absorption line due to the destructive quantum interference between two transitions in a three-level system. Using EIT in semiconductor quantum dots (QDs) is the way to engineering the material dispersion curve (i.e., refractive index as a function of frequency). Slowing down the group velocity is depended on creating quantum interference between a certain electronic states of the QDs via pumping the system by a strong controlling optical laser beam. By virtue of the Kramers-Krönig relations EIT absorption reduction is associated with a large positive slope of the refractive index. The resulting effect is a greatly reduced group velocity in the vicinity of resonances. Hence, the optical pump field can modify the real and imaginary parts of the refractive index of the medium seem by the signal beam. In "slow-light" techniques an external optical field (the "control field") is used to change an opaque medium to become transparent near the resonance. Under these considerations, a weak optical field (the "signal field") at a particular frequency and polarization can then propagate without loss but with a reduced group velocity. Associated with the slow light phenomena, the signal will be spatially compressed, which allows a signal pulse to be almost completely localized in the atomic medium [10].

Semiconductor based devices have some characteristics which make it more significant compared with gas- or solid-state-based ones. There are some examples: semiconductor transistors versus vacuum tubes, and diode lasers versus gas lasers, etc. [11]. The most important advantages includes compactness, monolithic integration and low power consumption. Experimental results of a slow-down factor of 10^7 have been reported using the EIT mechanism in a gas cell at 350 K [10] and cold cloud of sodium atoms [12], or solid-state systems such as Pr doped Y_2SiO_5. However, the transmission bandwidths obtained in these systems are too narrow (about 50–150 KHz) for optical buffers. Semiconductor structures such as quantum wells and QDs may offer more broadening transmission bandwidths (about a few GHz) at the cost of a smaller SDF

and with EIT buffers operating at room temperature [11]. A slowdown group velocity devices with transport bandwidth of tens kiloHertz is not appropriate for optical buffer applications [12].

In this paper, the maximum obtainable SDF (compared with disk quantum dot Ref.[13]) , S , which it is a measure of the group-velocity reduction, was examined. The SDF is a figure of merit relevant for optical storage. We use proper parameters of strained QDs from our electronic band structure model using COMSOL Multiphysics software and homemade Matlab codes for estimating SDF. The present study is based on the assumption that the medium is homogeneous.

2. Theoretical model

2.1 Light-matter interaction

A graphical scheme of three level system and the related parameters for EIT process in a QD is shown in Fig. 1. In this ladder order, only $|1\rangle \leftrightarrow |2\rangle$ and $|2\rangle \leftrightarrow |3\rangle$ are dipole allowed with energy separation of $\hbar\omega_{21}$ and $\hbar\omega_{32}$, respectively. ω_s and ω_p are the optical angular frequencies of the signal and the control laser beams, respectively. From the density matrix $\left(\frac{\partial\rho}{\partial t}\right)_{nm}$ theory, the optical dielectric constant experienced by the signal beam can be derived as follows:

$$\left(\frac{\partial\rho}{\partial t}\right)_{nm} = -(i\omega_{nm} + \gamma_{nm}) - \frac{i}{\hbar}\left[\hat{V},\hat{\rho}\right]_{nm} \qquad (1)$$

$$V_{nm} = -\frac{1}{2}\mu_{nm}E(\omega) + c.c., \qquad (2)$$

where γ_{nm} is the dephasing linewidth, and $\hbar\omega_{nm}$ is energy separation between states $|n\rangle$ and $|m\rangle$. μ_{nm} is the dipole moment. The electric field $E(\omega)$ includes the signal(E_s) and pump (E_p) is expressed as

$$E(\omega) = E_s e^{-i\omega_s t} + E_p e^{-i\omega_p t} \qquad (3)$$

The first-order optical susceptibility seen by the signal, $\chi(\omega_s)$, is expressed as [13]:

$$\chi(\omega_s) = \chi'(\omega_s) + i\chi''(\omega_s)$$

$$\chi'(\omega_s) = \varepsilon_b + \frac{U_{21}}{\hbar}\frac{\gamma_{31}{}^2\Delta_s - (\Delta_s+\Delta_p)[\Omega_p^2 - \Delta_s(\Delta_s+\Delta_p)]}{[\Omega_p^2 + \gamma_{21}\gamma_{31} - \Delta_s(\Delta_s+\Delta_p)]^2 + [\gamma_{21}(\Delta_s+\Delta_p) + \gamma_{31}\Delta_s]^2} \qquad (4a)$$

$$\chi''(\omega_s) = \frac{U_{21}}{\hbar}\frac{\gamma_{31}(\Omega_p^2 + \gamma_{21}\gamma_{31}) + \gamma_{21}(\Delta_s+\Delta_p)^2}{[\Omega_p^2 + \gamma_{21}\gamma_{31} - \Delta_s(\Delta_s+\Delta_p)]^2 + [\gamma_{21}(\Delta_s+\Delta_p) + \gamma_{31}\Delta_s]^2}, \qquad (4b)$$

where ε_b is a background dielectric constant.

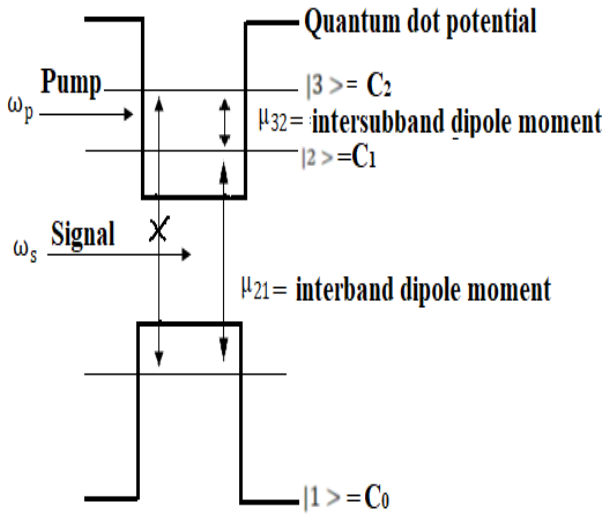

Fig. 1 Schematic diagram of the potential profile of semiconductor QD system. C_o=the heavy-hole ground state, c_1= the conduction band ground state, and c_2 = the first excited state of conduction band[13].

If both the signal and pump detuning vanishes, the SDF has an analytical form as follows, [13]:

$$SDF = \left[\frac{\varepsilon_b + \sqrt{\varepsilon_b^2 + \varepsilon_r^2}}{2}\right]^{1/2}\left[1 + \frac{\hbar\omega_s}{2\sqrt{\varepsilon_b^2+\varepsilon_r^2}}\frac{U_{21}(\Omega_p^2 - \gamma_{31}^2)}{\hbar^2(\gamma_{31}\gamma_{21} + \Omega_p^2)^2}\right] \qquad (5)$$

where

$$\varepsilon_r(\Omega_p^2) = \frac{U_{21}}{\hbar\left[\gamma_{21} + \frac{\Omega_p^2}{\gamma_{31}}\right]} \qquad (6)$$

and

$$I_p = \left(\frac{c}{\sqrt{\varepsilon_b}}\right)\varepsilon_o\varepsilon_b\left|E_p\right|^2 \quad (7)$$

where I_p is the pump power density, and

$$U_{21} = \Gamma|\mu_{21}|^2\frac{(f_1-f_2)}{V\varepsilon_o} \quad (8)$$

$$\Omega_p^2 = |\mu_{32}|^2\frac{I_p}{4\hbar^2 c\varepsilon_o\varepsilon_b} \quad (9)$$

U_{21} is the oscillator strength of the signal beam, Ω_p^2 is the launched pump power density, f_1 and f_2 are Fermi–Dirac occupation factors and for a passive undoped QD, $f_1 \sim 1$ and $f_2 \sim 0$, V is the volume of a single QD, μ_{21} and μ_{32} are the interband and intersubband dipole moments, c the speed of the light in vacuum.

2.2 Conical Quantum Dot System CQD

In this section, we tend to determine the bound electron and hole eigenstates through the numerical simulation of COMSOL software based on Finite Element Method (FEM). We consider an InAs conical QD with variable radius R and height z_o=3.5nm established on a wetting layer of thickness d=1.3 nm and embedded in cylindrical matrix GaAs barrier with radius R=12.5 nm, height z=100 nm. Since the CQD with WL is rotationally symmetric, the problem has been reduced to a two dimensional one. Hence, the wave function is written as

$$\psi(r) = \phi(r,z)\,e^{il\varphi}, \quad (10)$$

where $l = 0, \pm1, \pm2, \ldots$ is the orbital quantum number obtained by applying the periodic boundary condition. Then the Schrödinger equation in the cylindrical coordinates has the form:

$$-\frac{\hbar^2}{2\mathrm{m}}\left(\frac{1}{\mathrm{r}}\frac{\partial}{\partial \mathrm{r}}\left(\mathrm{r}\,\frac{\partial}{\partial \mathrm{r}}\right)+\frac{\partial^2}{\partial \mathrm{z}^2}-\frac{l^2}{\mathrm{r}^2}\right)\phi_l(\mathrm{r},\mathrm{z}) + \mathrm{V}(\mathrm{r},\mathrm{z})\,\phi_l(\mathrm{r},\mathrm{z}) = E_l\,\phi_l(\mathrm{r},\mathrm{z}), \quad (11)$$

where V is the potential energy, E_l is the energy eigenvalue, and ϕ_l is the envelope quantum mechanical wave function. In order to solve Eq. (11), it must be transformed to a generalized form of a coefficient partial differential equation used by COMSOL as follows:

$$\boldsymbol{\nabla}.(-c\boldsymbol{\nabla}u - \alpha u + \gamma) + au + \boldsymbol{\beta}.\boldsymbol{\nabla}u = d_a\lambda\, u \quad (12)$$

where the nonzero coefficients are: d_a is a damping coefficient, $d_a = 1$, c is the diffusion coefficient, $c = \frac{h^2}{(8\pi^2 m_e)}$, a is the conservative flux convection coefficient, $a = \left[\frac{h^2}{8\pi^2 m_e}\right]\frac{l^2}{r^2} + V$, $\boldsymbol{\beta}$ is the convection coefficient, $\beta_r = \left(\frac{-h^2}{8\pi^2 m_e}\right) * \frac{1}{r}$, α is the absorption coefficient, γ is the conservative flux source term, $\alpha = \gamma = 0$, and $\lambda = E_l$.

Indeed, the solutions of Eq. (12) is obtained for $\ell = 0$. The expression of the transition energy, E_{tr}, is written as follows:

$$E_{tr} = E_g + E_{c1} + E_{HH} \quad (13)$$

Where: E_g is the energy gap, E_{c1} is the quantization energy of the electrons and E_{HH} is the quantization energy of the holes.

3. Results and Discussions

In this paper, we report the dependency of the SDF of conical InAs QDs embedded in GaAs matrix on its radius and pump radiation intensity. A more realistic finite height potential barrier appropriate for experimental situation is employed. For CQDs with its wetting layer, the Eigenenergies, envelop functions, electric dipole moment matrix elements, relative linear refractive index, linear absorption coefficient and SDF are calculated versus the conical radius and light pump intensity. The wetting layer which is usually ignored in the previous articles [14] is included in this work. The strain field effect is ignored in this model. To solve the differential Eq. (11) numerically, the FEM of COMSOL Multiphysics has been used. To carry out our simulations, we discretized the structure area by triangular finite elements network. The mesh was refined near the QD and WL boundaries. The effective electron mass was set

to0.023 m_e for InAs and 0.067 m_e for GaAs [14], where m_e is the free electron mass. Also, the height of potential barrier was set as V=0.697eV.

3.1 Eigenfunctions and Eigenenergies calculations

In this subsection, we investigate the effects of radius on the electronic states of 3D conical-shaped QDs in details and wave functions associated with levels. The effect of radius on eigenvalue of CQD is studied in the range of (12-20) nm for 5.65 nm height and wetting layer thickness of 1.3 nm. The energy eigenvalues of electrons in the C.B are corresponding to the excited states of the three level ladder systems are shown in Fig. 2 for conduction band and Fig. 3 for valance band. Fig. 2 shows the ground state (lower) and first excited state (upper) energy eigenvalues versus the CQD radius. The Eigenenergies are almost changed linearly with the radius since the corresponding envelope functions are almost confined inside the CQD. Also, the same conclusion is valid for holes in valance band as indicated in Fig. 3.

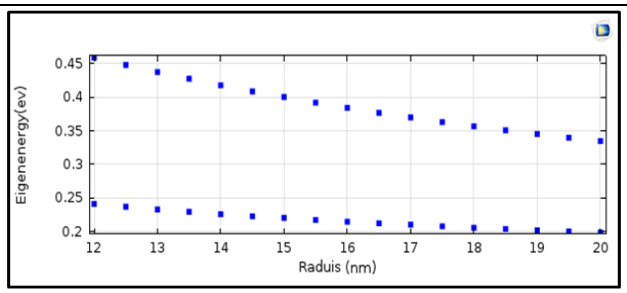

Fig. 2 Energy eigenvalues of electrons in the C.B as a function of CQD radius.

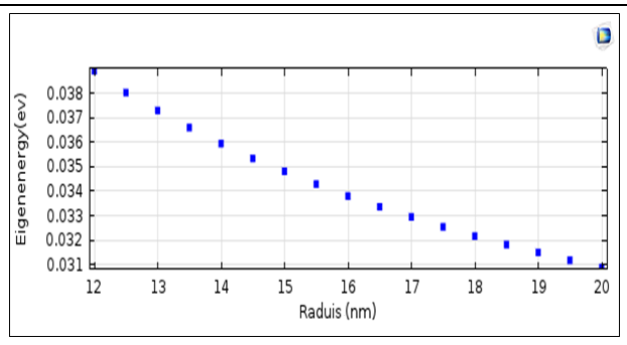

Fig. 3 Hole energy eigenvalues in the V.B as a function of CQD radius.

Fig. (4) show the one dimensional plot of probability density of normalized envelop wave functions corresponding to the ground and first three excited states in CB at two values of cone radius. The results show localization of ground state envelope function in CQD, whereas the first excited state has some expansion in the wetting layer as viewed in two and three dimension plots of Figs. (5-7). This situation is remains unchanged with increasing the cone radius. This picture actually will effect on electric dipole moments and the related optical properties.

The effects of changing radius on the energy transition ΔE between the hole and electron ground states can be understood with a simple analytical model. This transition has two contributions: strain and confinement. The strain is less at the band edges and affects the energy gap E_g, while the confinement increases the minimum allowed energy of electron E_{c1} and hole E_{HH} with respect to the band edges [15]. We can observe from the results obtained that the energy decreases with the increase of radius and this is consistent with the results of previous research [14].

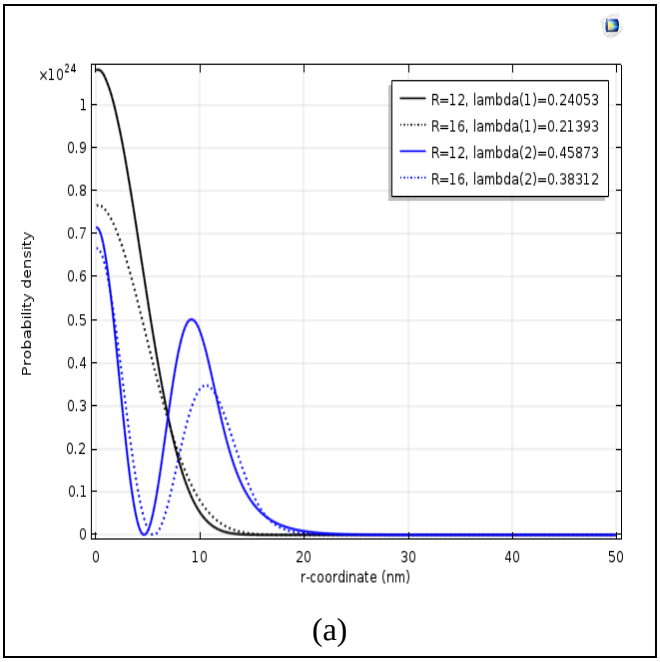

(a)

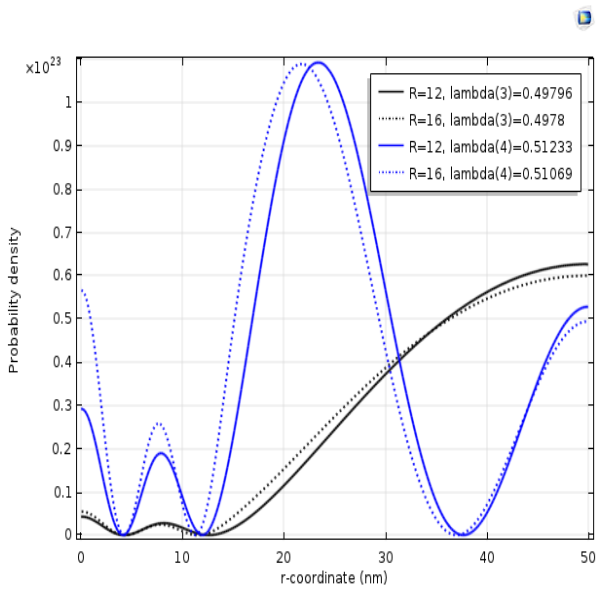

(b)

Fig. 4 One dimensional plot of the probability density uu^*in CQD, (a) 1st and 2nd eigen function, and (b) 3rd and 4th eign functions.

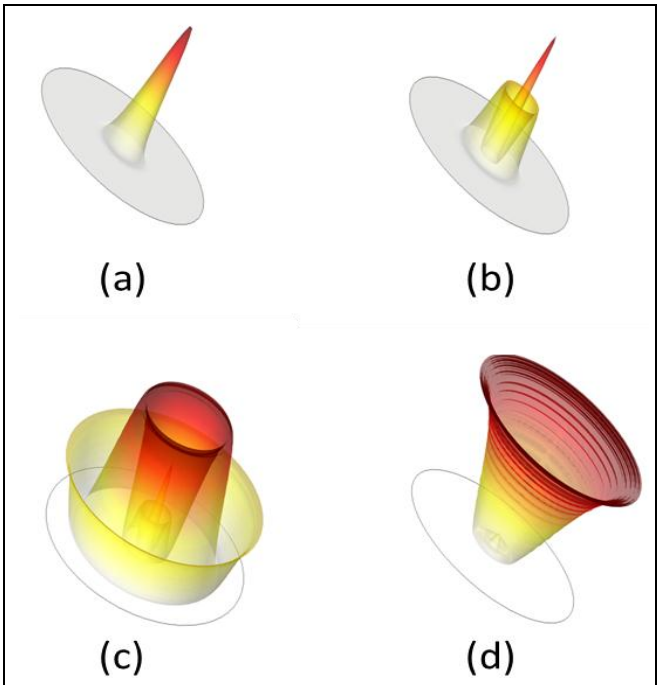

Fig. 5 Two dimensional plot in $r\varphi$ plane of the probability density uu^*in CQD, (a) first (b) second (c) third (d) fourth eigen function.

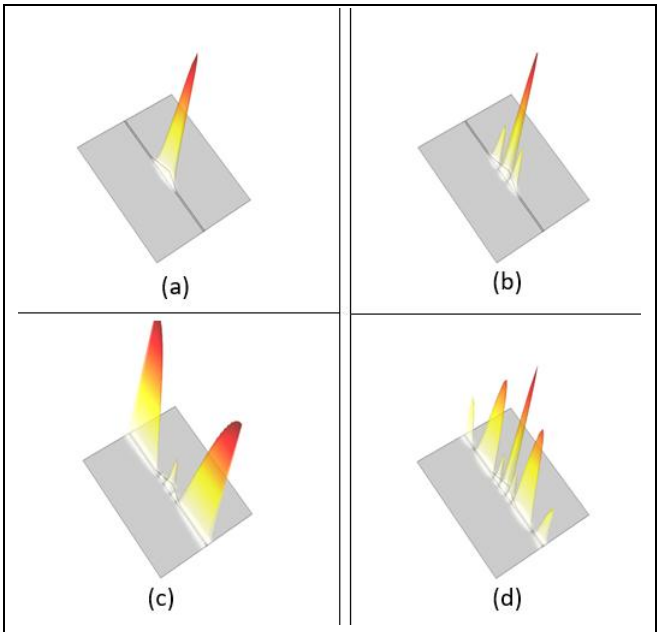

Fig. 6 Two dimensional plot in rz plane of the probability density uu^*in CQD, (a) first (b) second (c) third (d) fourth Eigenfunction.

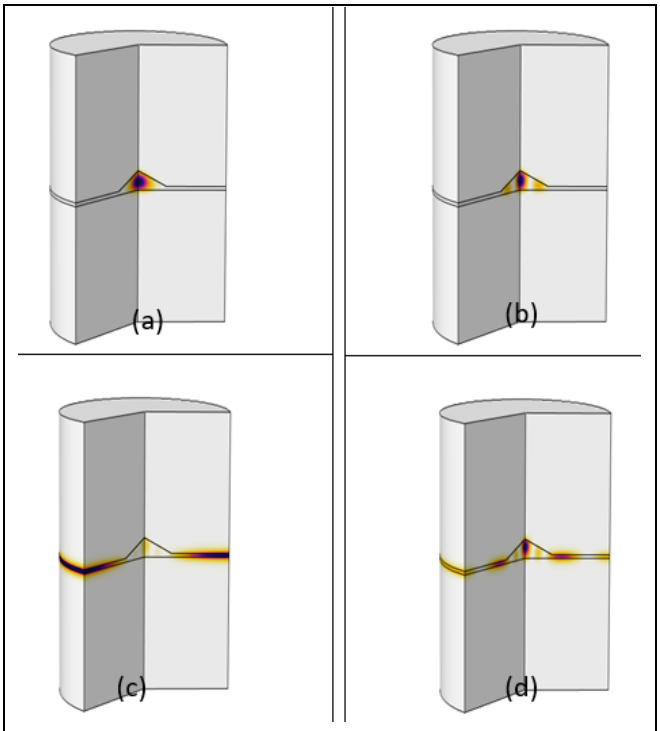

Fig. 7 Three dimensional plot of the probability density uu^*in CQD, (a) first (b) second (c) third (d) fourth eigen function.

3.2 Dipole moment calculations

Assuming a linear z-polarized electric field propagating along r direction, the intersubband dipole moment between the ground state level

$|2\rangle$ and the first excited state level $|3\rangle$ of the conduction band is given by

$$\mu_{32} = \langle \emptyset_3(r)|ez|\emptyset_2(r)\rangle \quad (14)$$

where e is the unit charge, and $|z|$ is the distance.

The controlling pump light should be chosen parallel to the QD plane in order to obtain maximum coupling between the pump beam and the $|3> \leftrightarrow |2>$ transition. The calculated intersubband dipole moment in the transverse direction is 24.2 eÅ when the radius and the height are 9 nm and 3.5 nm, respectively. Recall that the intersubband dipole moment is dependent on the radius of a QD, it calculates by using Comsol software.

Furthermore, the inter-band dipole moment can be expressed in terms of the momentum matrix element and the superposition integral of the wave functions as follows

$$\mu_{21} = \frac{e}{m_o \omega_s} \xi \, \langle u_c(r)|p|u_v(r)\rangle \, \langle \phi_2(r)|\phi_1(r)\rangle \quad (15)$$

where $u_c(r)$ and $u_v(r)$ are periodic parts of the ground state for the electron and the hole, respectively; and ξ is an enhancement factor due to exciton effects.

$$\langle u_c(r)|p|u_v(r)\rangle = \left(\frac{e}{2E_{tr}}\right)^2 \frac{E_g(E_g+\Delta_0)}{(E_g+2\Delta_0/3)m_c} \quad (16)$$

where: Δ_0 is the spin-splitting, and m_c is the electron effective mass. The parameters used in the study of inter-band dipole moment are indicated in the following table.

Table 1

parameter	Value
Enhancement factor (ξ)	4
Bulk band gap energy ($E_{g(InAs)}$)	0.42 eV
Bulk band gap energy ($E_{g(GaAs)}$)	1.52 eV
Spin-splitting ($\Delta_{0(InAs)}$)	0.48 eV
Spin-splitting ($\Delta_{0(GaAs)}$)	0.34 eV

The overlap integral of Eq. (15) ($\langle \phi_2(r)|\phi_1(r)\rangle$) was computed using the Comsol software. In general, a large inter-band dipole moment increases the SDF. The value of μ_{21}/e =4.5 eÅ will be used below in the calculation of group velocity reduction factor.

From Table 2, it is clearly shown that the intersubband dipole moment μ_{32} grows with increasing the CQD radius, since both ground and first excited states are completely confined inside the QD which leads more overlapping between them.

Table 2 Calculated inter-band (μ_{21}) and intersubband (μ_{32}) dipole moments for CDQ of 5.65 nm height.

Radius (nm)	μ_{21}/e (A)	μ_{32}/e (A)
12.0	5.40	32.4
12.5	5.61	36.5
13.0	5.75	36.2
13.5	5.94	38.6
14.0	6.14	40.8
14.5	6.36	43.7

3.3 Effect of pump density

The damping rates γ_{21} and γ_{31} (inverse of the dephasing times) are connected with the linewidths of the QD states, which are governed by several physical processes including carrier–phonon scattering, radiative recombination and exciton–phonon scatterings, among which the exciton–phonon scattering is dominated. The maximum achievable SDF is inversely proportional to the linewidth of a QD [13]. According to the experimental observations, a single QD has a dephasing time of several tens of picoseconds between 50 and 80 K [6, 13].

Fig. 8 show the normalized absorption spectra and refractive index calculated from the first-order susceptibility χ of the signal beam corresponding to imaginary and real parts of χ, respectively, at four different values of pump intensity field $\Omega_p = 0\gamma_{21}$ (blue), $2\gamma_{21}$ (green), $3\gamma_{21}$ (red), and $6\gamma_{21}$ (cyan), which are calculated using Eq. (4). In this figure, Δ_s and Δ_p are detuning frequencies for the signal and pump controlling beams, respectively, and

Ω_p is the Rabi frequency of the pump field. We have assumed Δ_p = 0 for maximum EIT effect which illustrate a typical EIT condition, and γ_{31} = $2\gamma_{21}$ since the excited electron state experiences more dephasing rate than the ground electron state does. The splitting of the second level $|2\rangle$, due to strong coupling field, the signal is clearly seen by two peaks in χ''. The magnitude of the level splitting is equal to $2\Omega_p$.

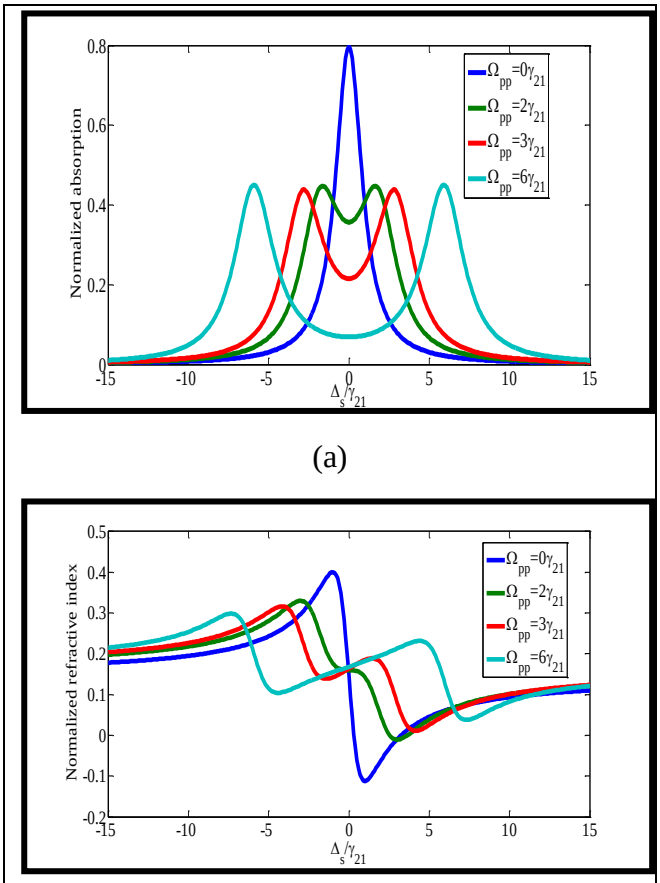

Fig. 8 Absorption (χ'') and Refractive index (χ') as a function of normalized signal detuning, (a) and (b), respectively, experienced by the signal for different values of Ω_p when Δ_p = 0 and γ_{31} = 2 γ_{21}; Δ_s and Ω_p are normalized to γ_{21}.

The maximum SDF is found at the frequency for which the slope of the refractive index is largest. Notice that the SDF obtained away from resonance is given by the background refractive index. The slope of the refractive index at zero detuning of the signal beam becomes nearly zero, when the pump power density reaches the value of 2 γ_{21}, and, the SDF approaches unity. The slope of the refractive index spectrum becomes positive and the group velocity starts to decreases, when we raise the pump power density. At a specific pump power density, the slope of the refractive index or the SDF reaches a maximum value, as shown in Fig. 8 at $\Omega_p = 3\gamma_{21}$ (red curve). If the pump power density further raised, the slope of the refractive index begin to reduce again due to increasing the transparency window experienced by the signal beam. Then, the group velocity reduction due to EIT are shown a maximum at a specific pump power density, which agrees with the experimental observations [16]. As is seen from Fig. 8 at $\Omega_p = 3\,\gamma_{21}$ in which the maximum group velocity SDF is obtained, the bandwidth is comparable to the linewidth γ_{21}. The transparency bandwidth can be raised further via rising the pump power density, but with the cost of lowering the group velocity SDF, as can be seen from Fig. 8 at $\Omega_p = 6\,\gamma_{21}$.

Investigating the group velocity SDF as a function of pump coupling intensity based on Eq. (5) for three various linewidth values of $\hbar\gamma_{21}$ = 1.6, 6.6, and 26.5 μeV is depicted in Fig. 9 using the material parameters defined above with the assumption of $\gamma_{31} = 2\gamma_{21}$. Also, the signal wavelength is 1.36 μm, ε_b = 13, μ_{21} /e = 4.5 Å, and μ_{32} /e = 24.2 Å. Each CQD has a radius of 9 nm and a height of 3.5 nm. The optical confinement factor, $\Gamma = 6 \times 10^{-3}$ and a QD surface density of $4 \times 10^{10}\text{cm}^2$ is used. The selected three various linewidth values were agreed to 2.5, 10, and 40 Gbps bandwidth. The transportation window is determined through the ratio between the Rabi frequency and the linewidth. Fig. 9 shows that the studied group velocity decrease factor for γ_{21} = 26.5 μeV is about 556.1. This decrease factor would be appropriate for optical buffers in all-optical packet-switched networks.

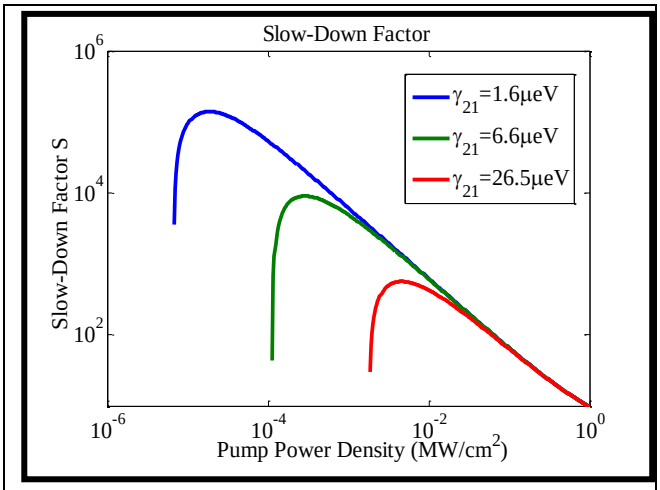

Fig. 9 The group velocity SDF as a function of the pump power density at three linewidth values: $\hbar\gamma_{21}$, 1.6, 6.6, and 26.5 μeV at $\gamma_{31} = 2\gamma_{21}$.

3.4 SDF as a function of CQD radius

By using Eqs. (14) and (15) we calculated the interband (μ_{21}) and intersubband (μ_{32}) dipole moment at different CQD radius to estimate the SDF as a function of radius. The results are appeared in table 2. Fig. 10 shows the graph of the SDF of a set of six different radius starts with 12 nm and ends at 14.5 nm. Based on the obtained results, it can be said when the radius of CQD is decreased, the slope of real part of refractive index curve increases and therefore, a bigger SDF is achieved. In this paper a maximum SDF equal to 9351 can be achieved for radius of 12 nm and height of 5.56 nm. Of course, the radius decrease causes frequency shift too [8].

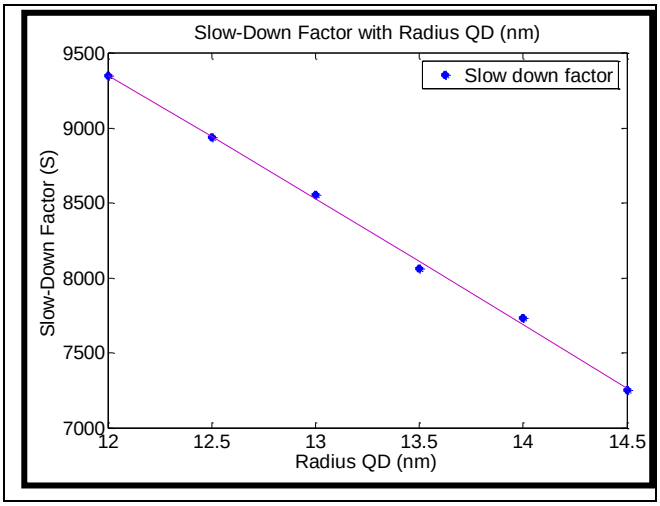

Fig. 10 The group velocity SDF as a function of CQD radius.

4. Conclusion

We have investigated of a semiconductor all-optical buffer based on EIT effect in three level ladder CQD systems. We describe the dynamics of the medium by Bloch equations with transition matrix elements calculated for CQD established on a wetting layer. We recognized the formulation and conditions necessary to obtain a large SDF. Since the light pulses can be slowed down significantly with a small dispersion, making it desirable for optical buffer devices with a variable storage time. The effects of the dephasing rate on the SDF of the signal light are investigated since the main factor of the dephasing is from exciton–phonon scattering which is limited by the radiative recombination [17]. We also expect that energy configuration and further optimization in device design can lead to significantly raised SDF. We believe an optical buffer would serve as a critical catalyst to move new design and applications in optical networks, communications, and signal processing.

REFERENCES

[1] Y. Fu, F. Ferdos, M. Sadeghi, S.M. Wang and Larsson, "Broadening of photoluminescence by nonhomogeneous size distribution of self-assembled InAs quantum dots", Appl. Phys., 92, 3089, 2002.

[2] G. C. Sherman, K. E. Oughstun, "Energy-velocity description of pulse propagation in absorbing, dispersive dielectrics", J. Opt. Soc. Am. B., 12, 229-247, 1996.

[3] COMSOL Multiphysics Model Library copyright, 1998-2008 by COMSOL AB.

[4] RF Module User's Guide. 1998-2012 COMSOL-Protected by U.S. Patents

7, 519, 518; 7, 596, 474; and 7, 623, 991. Patents pending.

[5] D. Mogilevtsev, E. Reyes-Gomez, S. B. Cavalcanti, and L. E. Oliveira, "Slow light in semiconductor quantum dots: Effects of non-Markovianity and correlation of dephasing reservoirs", Phys. Rev., B 92, 235446, 2015.

[6] B. Choupanzadeh, H. Kaatuzian, R. Kohandani, S. Abdolhosseini, "Simulation and characteristics improvement of quantum dot slow light devices by geometrical dimension alteration", Opt. and Phot. J., 6, 114-119, 2016.

[7] B. Choupanzadeh, H. Kaatuzian, R. Kohandani, S. Abdolhosseini, "Simulation and Characteristics Improvement of Quantum Dot Slow Light Devices by Geometrical Dimension Alteration", Opt. Photo., 6, 114-119, 2016.

[8] M. S. Bigelow, N. N. Lepeshkin and R.W. Boyd, "Superluminal and Slow Light Propagation in a Room-Temperature Solid", Science, 301, 200-202, 2003.

[9] H. Kaatuzian, H. S. Kojori, A. Zandi, M. Ataei,"Analysis of Quantum Well Size Alteration Effects on Slow Light Device Based on Excitonic Population Oscillation", Opt. Quant. Electron., 45, 947-959, 2013.

[10] D. F. Phillips, A. Fleischhauer, A. Mair, and R. L. Walworth, "Storage of light in atomic vapor", Phys. Rev., 5, 783-786, 2001.

[11] D. Mogilevtsev, E. Reyes-Gomez, S. B. Cavalcanti, and L. E. Oliveira, "Slow light in semiconductor quantum dots: Effects of non-Markovianity and correlation of dephasing reservoirs", Phys. Rev. B, 92, 235447-235455, 2015.

[12] A.V. Turukhin, V. S. Sudarshanam, and M. S. Shahriar, "Observation of Ultraslow and Stored Light Pulses in a Solid", Phys. Rev. 88, 023602-023606, 2002.

[13] J. Kim, S. L., Chuang1, P. C. Ku, and C. J. Chang-Hasnain, "Slow light using semiconductor quantum dots", J. Phys., Condens. Matter, 16, 3727–3735, 2004.

[14] G. Rezaei, Z. Mousazadeh, B. Vaseghi," Nonlinear optical properties of a two-dimensional elliptic quantum dot", Phys. E, 42, 1477–1481, 2010.

[15] A. Benahmed1, A. Aissat1, M. A. Benammar, "Optical Transitions in Quantum Dots", Inter. J. Phys., 2, 109-111, 2014.

[16] P. C. Ku, C. J. Chang-Hasnain and S. L. Chuang, "Slow light in semiconductor Heterostructures", J. Phys. D: Appl. Phys., 40 , 93–107, 2007.

[17] M. Bayer and A. Forchel, "Temperature dependence of the exciton homogeneous linewidth in In0.60Ga0.40As/GaAs self-assembled quantum dots", Phys. Rev. B 65 041308, 2002.